scientific reports

Check for updates

OPEN

Investigating the PI3K/AKT/mTOR axis in Buzhong Yiqi Decoction's anti-colorectal cancer activity

Song Qiao[1], Xiaolong Li[2], Shangzhen Yang[1], Hua Hua[1], Chengtao Mao[1] & Wanling Lu[1]✉

Buzhong Yiqi Decoction (BZYQD) is a traditional Chinese medicine renowned for its anti-colorectal cancer (CRC) properties. However, the bioactive components and mechanisms of BZYQD against CRC remain unknown. In this study, LC-MS was used to analyze the chemical composition of BZYQD. Next, the network pharmacology and molecular docking was used to investigate the core components and targets of BZYQD against CRC. Finally, we experimentally validated the potential mechanism of BZYQD against CRC through in vitro studies. Our results identified 26 chemical components in the BZYQD; 75 "hithubs" targets were screened by network pharmacology, and mainly involving pathways such as including pathways in cancer, P13K-Akt signaling pathway, proteoglycans in cancer, kaposi sarcoma-associated herpesvirus, and lipid and atherosclerosis signaling pathways. Based on the number of "hithubs" targets in the key pathways, the two most critical targets including AKT1 and PIK3CA were selected. The component-target network results indicated that astragaloside IV, gancaonin A, quercetin, poricoic acid A, and licoisoflavanone are key anti-CRC components in BZYQD. Molecular docking showed a strong binding affinity between these components and targets. The phosphoinositide 3-kinase (PI3K)/protein kinase B (AKT) signaling pathway emerged as the primary target of BZYQD. Further in vitro studies confirmed that BZYQD's anti-CRC activity is mediated through the PI3K/AKT/mTOR axis and influences macrophage polarization. BZYQD exerts its therapeutic effects on CRC through multiple components, targets, and pathways. Our study elucidates the effective components and molecular mechanisms of BZYQD in CRC treatment and provides preliminary validation through molecular docking and experimental studies.

Keywords Buzhong Yiqi Decoction, Colorectal cancer, LC-MS, Network pharmacology, PI3K/AKT/mTOR pathway

Colorectal cancer (CRC) ranks third in both incidence and mortality among malignant diseases[1]. The U.S. Department of Health and Human Services reported that CRC was the second leading cause of cancer-related death[2]. According to the American Oncology Society, there will be 147,950 new CRC diagnoses and approximately 53,200 deaths by 2020[3]. Over the past thirty years, the incidence of CRC has been increasing in China, with a persistent upward trend. Official statistics from 2020 ranked CRC as the second most common cancer in terms of incidence and fourth in mortality[4]. Currently, 5-fluorouracil and other fluoropyrimidines are commonly used in the treatment of CRC; however, their long-term use is often limited due to adverse side effects. Therefore, it is crucial to explore safer and more effective methods for the prevention and treatment of CRC.

Traditional Chinese medicine (TCM) offers extensive experience and unique benefits for CRC treatment[5]. Buzhong Yiqi Decoction (BZYQD), developed by the renowned physician Li Dongyuan, consists of ingredients such as Astragalus membranaceus, ginseng, Atractylodes macranthoides, Radix Glycyrrhizae, Bupleurum, Cimicifugae, Angelica, and Pericarpium Citri Reticulatae[6,7]. It has a medicinal history of over 700 years in China and is also widely utilized in South Korea, Japan, and beyond. Modern pharmacological research has demonstrated that BZYQD can enhance immunity, regulate gastrointestinal function, and exhibit anti-inflammatory and anti-tumor properties[8,9]. As an adjunct therapy for CRC, BZYQD has been shown to alleviate clinical symptoms, enhance quality of life, and reduce the likelihood of tumor recurrence[10]. Numerous randomized controlled trials in China have indicated that combining BZYQD with chemotherapy notably improves patient symptoms and

[1]Department of Oncology and Hematology, Xijing 986 Hospital, No. 269 Youyi East Road, Beilin District, Xi'an 710054, Shaanxi, China. [2]Radiotherapy 1 Ward, Shaanxi Provincial Cancer Hospital, No. 309, Yanta West Road, Yanta District, Xi'an, Shaanxi, China. ✉email: asd20241231024@163.com

immune function over chemotherapy alone[8]. However, the components and mechanisms by which BZYQD treats CRC remain underexplored.

The field of network pharmacology combines systems biology and network informatics, and has gained popularity in the past few years[11]. A systems biology approach to disease postulates that complex diseases do not originate from a single mutation in a gene, but rather from a number of mutations that disrupt the balance within biological networks[12]. Network pharmacology examines this balance and enables the analysis of how multi-component drugs impact the human body at a systemic level[12]. This approach aids in identifying therapeutic targets for drug constituents, improving drug efficacy, and minimizing side effects[13]. Molecular docking allows for the atomic-level modeling of interactions between molecules and proteins, predicting ligand-receptor conformations and calculating parameters[14].

In this study, LC-MS was used to analyze the chemical components of the BZYQD. Subsequently, network pharmacology and molecular docking were utilized to investigate the active components and mechanisms of BZYQD. Additionally, preliminary validations were conducted through cellular experiments.

Materials and methods

Drugs and reagents

BZYQD is composed of Astragalus membranaceus, ginseng, Atractylodes macrocephala, Radix Glycyrrhizae, Bupleurum, Cimicifuga, Angelica, and Pericarpium Citri Reticulatae. All herbs obtained from Xijing 986 Hospital. Analytically pure methanol, petroleum ether and acetonitrile were sourced from Tianjin Sifang Chemical Co., Ltd., China. Mass spectrometry pure methanol and acetonitrile were purchased from Thermo fisher, USA. Chromatographically pure formic acid was also procured from Thermo fisher, USA, DMSO was obtained from Tianjin Fuyu Fine Chemical Co., Ltd., China. We obtained fetal bovine serum (FBS) from Gibco (Grand Island, NY, USA), along with high-glucose DMEM and PBS from GIBCO Life Technologies. Protein detection using BCA and the preparation of SDS-PAGE gels were carried out with products from Sigma-Aldrich, while reverse transcription was performed using Vazyme Biotechnology (Nanjing, China). The antibodies utilized in our research, including GAPDH (AC001), PI3 Kinase P85 (A5441), AKT (A5523), mTOR(A11355), phospho-Pl3 Kinase p55-Y199 (AP1463), phospho-AKT-S473 (AP1208), and phospho-mTOR-S2448 (AP0115), were obtained from ABclonal Technology (Wuhan, China). Both IGF-1 and LY294002 were procured from Sigma Chemical.

The equipment used includes a Thermo Fisher U3000 UPLC(Thermo Fisher Company, USA), Thermo Fisher Q ExactiveTM Orbitrap MS(Thermo Fisher Company, USA), KQ-300E Ultrasonic Cleaner (Kunshan Ultrasonic Instrument Co., Ltd., China), Sartorius BSA124S Analytical Balance (Sartorius Company, USA), Neofuge 13R High Speed Refrigerated Centrifuge (Shanghai Lishen Scientific Instrument Co., Ltd., China), Milli-Q Integral Water Purification Pure Water System (Millipore Company, USA), and HH-4 Digital Display Thermostatic Water Bath Pot (Jintan Jereel Electric Appliance Co., Ltd., China).

Preparation of BZYQD

The above herbs of BZYQD were decocted with pure water for 2 times (1:10, first 2 h, second 2 h). The two water extracts were combined and filtered through gauze. The supernatant was concentrated to 1 L using a rotary evaporator. Additionally, the supernatant was frozen overnight at − 80 °C and then freeze-dried using a freeze-dryer to obtain freeze-dried powder. For in vitro experiments, the BZYQD powder was dissolved in the required concentration medium.

The preparation of sample solution is as follows: 100 mg of BZYQD was added to 5 mL of 95% methanol, vortexed for 1 min, and subjected to ultrasonic extraction for 20 min. The mixture was then centrifuged at 13,000 r/min for 15 min. The supernatant was collected and filtered through a 0.22 μm microporous membrane before analysis.

LC-MS conditions

LC conditions: the chromatographic column used was a Waters HSS T3 liquid chromatography column (2.1 mm × 100 mm,1.8 μm). The mobile phase consisted of 0.1% formic acid aqueous solution (A) and methanol (B). The column temperature was maintained at 40 ℃, with a flow rate of 0.20 mL/min, and an injection volume of 5 μL. The gradient conditions were as follows: 0 ~ 1 min,10% B;1 ~ 8 min,10% ~ 60% B;8 ~ 14 min,60 ~ 98% B; 14 ~ 15 min,98% ~ 10% B;15 ~ 16 min,10% B.

MS conditions: Data was collected using an ESI ion source in both positive and negative ion modes, with a data collection range of 50–1500 m/z. The ion spray voltages were 3.5 kV for positive mode and 2.5 kV for negative mode. The de-clustering voltage and inlet voltage were set to 70 V and 10 V, respectively. The collision gas, atomization gas, auxiliary heating gas, and curtain gas were set to 50, 50, and 35 psi, respectively. The solvent removal temperature was 320 °C. The fast data-dependent acquisition (DDA) method was used, with an intensity threshold of 5000, selecting the 15 ions with the highest intensity for mass spectrometry detection.

Analysis method: The data were analyzed using Compound Discoverer 3.1 (CD) software, employing online databases such as Chemspider, mzVault, and mzCloud for non-targeted searches of the mass spectrometry data. Information on sample name, retention time, molecular formula, mass-to-charge ratio, and corresponding ion intensity were obtained. A comprehensive analysis was conducted using an established local chemical composition database and the results from CD 3.1. Primary and secondary mass spectrometry information was extracted using Xcalibur 3.2 software (Thermo, USA), and the chemical components of BZYQD were further identified by combining diagnostic ions, fragment ions, literature data, and database information.

Network pharmacology analysis

Identification and screening of active chemical constituents in BZYQD

Using the traditional Chinese medicine systems pharmacology database (TCMSP, http://lsp.nwu.edu.cn/tcmsp.php), the active constituents of Astragalus membranaceus, ginseng, Atractylodes macrocephala, Radix Glycyrrhizae, Bupleurum, Cimicifuga, Angelica, and Pericarpium Citri Reticulatae were identified based on criteria of oral bioavailability (OB) > 30% and drug-likeness (DL) > 0.8.

Identification of potential target proteins for BZYQD and CRC

We explored potential targets of BZYQD in Homo sapiens using various online databases, including TCMSP (http://tcmspnw.com/), SwissTargetPrediction (http://swisstargetprediction.ch/), PharmMapper (http://www.lilab-ecust.cn/pharmmapper/), and PubMed database (https://pubmed.ncbi.nlm.nih.gov/), and merged with targets from the aforementioned sources, ensuring elimination of redundancy to compile the relevant targets of BZYQD. Additionally, we gathered disease target information pertinent to CRC from databases such as DisGeNET (https://www.disgenet.org/), GeneCards (https://www.genecards.org/), OMIM (https://omim.org/), and TTD (http://db.idrblab.net/ttd/). Utilizing the UniProt database (http://www.uniprot.org/) with a focus on Homo sapiens, we consolidated these targets and removed duplicates.

Construction of protein-protein interaction network

The protein interaction network was constructed by integrating the targets of BZYQD and CRC identified in our searches. Cytoscape software was employed to combine the interaction networks of the two sets of proteins. Through the CytoNCA, we obtained multiple attribute values and identified nodes with degree values exceedingly twice the median of all degree values as "hubs". Key interaction nodes between BZYQD and CRC were identified through three screening rounds, using criteria where degree, betweenness, and closeness were each at least equal to the median of all nodes. Finally, we constructed the protein-protein interaction network of BZYQD in relation to CRC treatment.

GO and KEGG pathway enrichment analysis

Enrichment analyses for KEGG pathways and GO biological processes were performed using the DAVID 6.7 database (https://david.ncifcrf.gov/). The selection criteria for KEGG pathway enrichment included pathways with both *p*-values and Benjamini values less than or equal to 0.05, with the top 15 pathways highlighted based on their count values. A GO enrichment analysis was conducted on three categories. Bioinformatics tools were used to visualize the analysis (http://www.bioinformatics.com.cn/), resulting in bubble charts and histograms.

Molecular docking

AKT1 (PDB ID: 6HHG) and PIK3CA (PDB ID: 2RD0) ternary crystal structures were identified from the Protein Data Bank (PDB). After removing water molecules from astragaloside IV, gancaonin A, quercetin, poricoic acid A, and licoisoflavanone, hydrogen atoms were added to prepare ingredients. Docking activity was determined based on the results of the docking calculations.

Cell assays

The colorectal cancer cell lines HCT116 were cultured in DMEM supplemented with 10% FBS and 1% penicillin (100 units/mL) and streptomycin (100 μg/mL). Cultures were maintained at 37 °C in a cell incubator under a 5% CO_2 atmosphere.

Cell proliferation assays

Cell viability was measured using the MTT assay (Sigma). The 5-ethynyl-2′-deoxyuridine (EdU) assays were performed with the Cell-Light EdU Apollo®488 in vitro kit from RiboBio, Guangzhou, China. In these experiments, cells were seeded into 48-well plates at a density of 5 × 103 cells/well and cultured for 24 h in medium without drugs. Following treatment with different concentrations of drugs for 24 h, a 50 M EdU solution was added to the media and co-incubated for 2 h. After fixing, the cells were stained with Apollo® staining solution, and imaged by fluorescence microscopy.

Cell migration assay

A wound healing assay was used to assess cell motility. Cells were seeded in a six-well plate at a density of 1×10^6 cells per well and incubated for 24 h in drug-free medium. After scratch wounds were created with a 20 μl pipette tip, each drug was applied to the wound for an additional 24 h. Cells were photographed before and after treatment. In Transwell migration assays, cell suspensions were prepared at 2.5×10^5 cells/ml in serum-free medium, with 100 μl added to the upper chamber. A fraction of each drug concentration was mixed with 10% FBS in the lower chamber, followed by paraformaldehyde fixation, crystal violet staining, and subsequent imaging of the extracts.

Immune effect of the BZYQD on TAMs in vitro

To investigate the immune effects of the BZYQD, TAMs were incubated with BZYQD for 8 h. The murine RAW264.7 macrophages were subjected to the following treatments: (1) 0.1% DMSO served as the control group. (2) LPS (10 ng/mL) and IFN-γ (20 ng/mL) were categorized as the M1 group. (3) IL-4 (20 ng/mL) were referred to as the M2 group. (4) BZYQD (165, 330, and 660 μM), were labeled as Con + BZYQD (165), Con + BZYQD (330), and Con + BZYQD (660), respectively. RAW264.7 cells in the logarithmic growth phase were seeded at a density of 2×10^5 cells/mL in 96-well plates and incubated overnight. The cells were then stimulated with LPS and IFN-γ to induce M1 differentiation, or with IL-4 to induce M2 differentiation. Concurrently, RAW264.7

cells were co-treated with BZYQD. After 24 h, cell viability was assessed using the MTT assay. Mean fluorescence intensity (MFI) of the cell surface molecules was assessed by flow cytometry (FCM). The TAMs were collected, washed twice with PBS (10 mM, pH 7.4), and then incubated with fluorochrome-labeled antibodies against CD86 and CD206, diluted in flow cytometry staining buffer. The expression levels of these markers on the TAMs were quantified. Data analysis was performed using FlowJo software (version 7.6). Additionally, cytokine concentrations in the supernatants of TAMs were measured using ELISA kits for mouse IL-6 and IL-10.

Western blot

Protein extraction was performed according to the total protein extraction kit instructions. The protein concentration of each sample was determined using the BCA assay kit (Thermo Fisher Scientific). Total proteins were separated by 10% SDS-PAGE, and subsequently transferred to a polyvinylidene fluoride (PVDF) membrane, which was blocked with 5% skim milk powder for 1 h. The membrane was incubated overnight with a primary antibody, followed by a room temperature incubation with a secondary antibody. The PVDF membrane was developed using exposure solution, and the gray values of the protein bands were quantified using ImageJ software. The analysis was conducted with GAPDH serving as the internal reference for determining the gray values of the protein bands.

Statistical analyses

Data are presented as mean ± standard error of the mean. Statistical evaluations were conducted using one-way analysis of variance along with Dunnett's multiple comparisons test, with a significance level set at $P < 0.05$.

Results

Chemical compositions of BZYQD

Through a literature review conducted on databases such as Web of Science, PubMed, CNKI, as well as online resources like TCMSP and TCMID, we established a chemical composition library for BZYQD. This library includes the names, molecular formulas, structural formulas, and precise molecular weights of each compound. Some compounds were supplemented with mass spectrometric fragment ion information sourced from the MassBank (http://massbank.eu) and PubChem (https://pubchem.ncbi.nlm.nih.gov/) databases. During the identification of chemical compositions, the primary and secondary mass spectrum data of the components in the localized component library were manually extracted and compared with mass spectrum information from the databases, ultimately leading to the identification of the chemical compositions. The total ion chromatograms of BZYQD in both positive and negative ion modes are illustrated in Fig. 1A and B, with a total of 26 compounds identified. Detailed information about these compounds is presented in Table 1.

Network pharmacology prediction

Identiffcation of targets of BZYQD against CRC

A total of 781 targets associated with BZYQD were identified using the TCMSP, Swiss Target Prediction, Pharmmapper, and PubMed databases. 3737 CRC-related targets were retrieved from the Digenet, Genecards, OMIM, and TTD databases. Two target networks were created by Cytoscape software (Fig. 2A) These networks comprised 781 nodes with 14,940 connections and 3,737 nodes with 75,448 connections, respectively (Fig. 2A). By merging these two networks, an overlapping network was generated, consisting of 653 nodes and 12,931 connections (Fig. 2A). Nodes with a degree value of at least double the median of all nodes were selected, resulting in a "hithub" network featuring 75 nodes and 1,815 connections. The nodes in "hithub" network were considered key targets in the interaction between BZYQD and CRC (Fig. 2A).

KEGG and GO pathway enrichment analysis

To investigate the potential mechanisms through which BZYQD treats CRC, a bubble diagram was created, as shown in Fig. 2B, highlighting several CRC-related signaling pathways, including pathways in cancer, P13K-Akt signaling pathway, proteoglycans in cancer, kaposi sarcoma-associated herpesvirus, and lipid and atherosclerosis signaling pathways. Notably, the PI3K/AKT signaling pathway emerged as the most significant. The results of the GO enrichment analysis (Fig. 2C) indicated that key targets involved in the interaction between BZYQD and CRC primarily participate in processes such as protein binding, identical protein binding, ATP binding, cytoplasm, cytosol, nucleus, signal transduction, positive regulation of transcription by RNA polymerase ll, phosphorylation.

Protein-protein interaction network

Based on the key targets and KEGG pathways related to BZYQD's treatment of CRC, a target-pathway network diagram was constructed using Cytoscape 3.7.2 software, as depicted in Fig. 2D. To analyze the core targets further (illustrated in Fig. 2E), the targets were ranked according to the number of pathways they were associated with. The findings revealed that AKT1 and PIK3CA were involved in numerous pathways, suggesting they may serve as core targets for BZYQD. At the same time, the network core compounds Astragaloside IV, gancaonin A, and quercetin mainly act on AKT1 and quercetin, poricoic acid A, and licoisoflavanone mainly act on PIK3CA.

Molecular docking

Using molecular simulation software (Discovery Studio 3.5), astragaloside IV, gancaonin A, and quercetin were docked with AKT1, while quercetin, poricoic acid A, and licoisoflavanone were docked with PIK3CA. Binding energy values less than 0 indicate the potential for spontaneous and stable binding between ligands and receptors, with lower values signifying higher affinity. As shown in Fig. 3, the docking binding energies of astragaloside IV, gancaonin A, quercetin, poricoic acid A, and licoisoflavanone with AKT1 and PIK3CA were all below

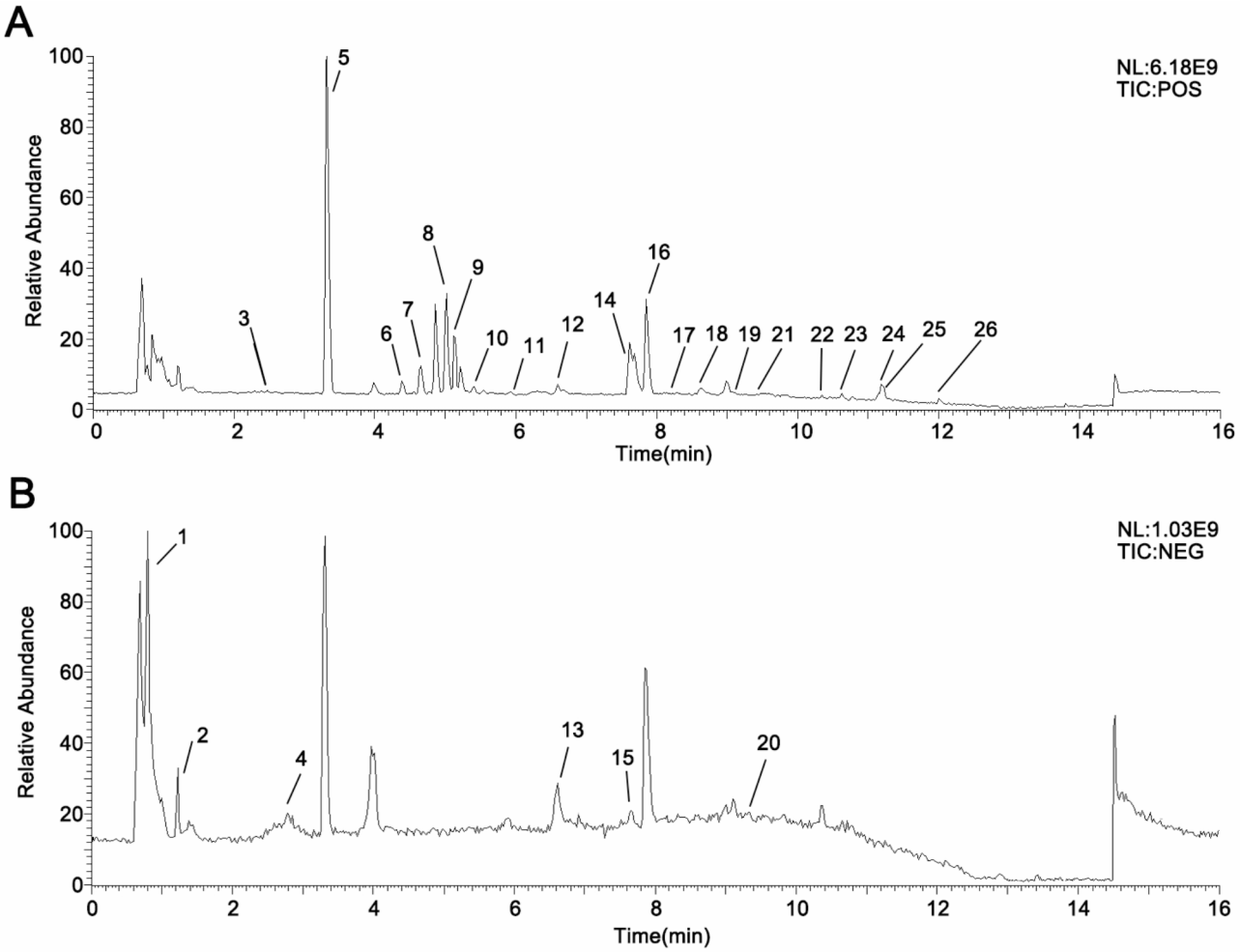

Fig. 1. Total ion chromatograms (TIC) of positive (**A**) and negative (**B**) ions in BZYQD.

zero, implying strong binding affinities. Specifically, astragaloside IV and gancaonin A exhibited high binding activities with AKT1, with binding energies of -5.64 and −7.49 kcal/mol, respectively (Fig. 3A-C). Similarly, quercetin and licoisoflavanone demonstrated high binding activities with PIK3CA, with binding energies of -7.30 and −6.48 kcal/mol, respectively (Fig. 3D-F). These findings support the therapeutic potential of BZYID in CRC treatment at the molecular docking level, suggesting that astragaloside IV, gancaonin A, quercetin, and licoisoflavanone may be key compounds contributing to the efficacy of BZYID.

BZYQD inhibits CRC cell proliferation and migration in vitro

The IC50 value of BZYQD was determined to be 329.7 μg/mL for HCT116 cells (Fig. 4A, B and $F_{5,30} = 45.137$, $P < 0.001$. Based on this, the concentrations of 165, 330, and 660 g/mL of BZYQD were selected as low doses, medium doses, and high doses, respectively. In vitro EdU assays confirmed that BZYQD significantly inhibited HCT116 cell proliferation (Fig. 4C, D and $F_{3,8} = 69.537$, $P < 0.001$). Additionally, wound healing and Transwell migration assays showed that BZYQD components significantly reduced the migration capability of HCT116 cells in vitro (Fig. 4E and F). These results suggested that BZYQD inhibits CRC cell proliferation and migration. Furthermore, we evaluated the IC50 values of the five active ingredients, revealing that the IC50 values for astragaloside IV, gancaonin A, quercetin, poricoic acid A, and licoisoflavanone were 101.9, 172.8, 160.2, 2090, and 9268 ng/mL, respectively (Supplemental Fig. 1), for HCT116 cells. All these compounds demonstrated inhibitory activity against HCT116 cells, with astragaloside IV, gancaonin A, and quercetin being particularly effective. These components form the primary material basis for BZYQD's anti-CRC activity.

BZYQD inhibits PI3K/Akt/mTOR signaling pathway activation

HCT116 colon cancer cells were treated with BZYQD at concentrations of 0, 165, 330, and 660 μg/mL for 24 h, followed by Western blot analysis to assess PI3K/AKT/mTOR levels. Results indicated that BZYQD dose-dependently inhibited the expression of p-PI3K ($F_{3,8} = 36.494$, $P < 0.001$), p-Akt ($F_{3,8} = 23.735$, $P < 0.001$), and p-mTOR (($F_{3,8} = 4.618$, $P < 0.05$, Fig. 5A and B), indicating inhibition of the PI3K/Akt/mTOR signaling pathway by BZYQD.

No	RT (min)	Name	Formula	ion	Cal. m/z	Mea. m/z	Error (ppm)	MS/MS
1	0.79	Citric acid	$C_6H_8O_7$	M-H	191.0197	191.0195	-0.605	41.0036
2	1.22	Isoferulic acid	$C_{10}H_{10}O_4$	M-H	193.0506	193.0504	4.479	133.0288
3	2.47	Isoflavanone	$C_{15}H_{12}O_2$	M + H	225.091	225.0915	2.194	225.0915, 121.0126
4	3.32	Naringenin	$C_{15}H_{12}O_5$	M-H	271.0611	271.0616	5.534	119.0487, 107.0125
5	3.33	Paeonol	$C_9H_{10}O_3$	M + H	167.0702	167.0706	1.971	149.0599, 121.0657
6	4.38	Nobiletin	$C_{21}H_{22}O_8$	M + H	403.1387	403.1385	0.531	355.0814, 342.1109
7	4.66	Aloe-emodin	$C_{15}H_{10}O_5$	M + H	271.0601	271.0606	1.845	153.0186, 119.0467
8	5.01	Astragaloside IV	$C_{41}H_{68}O_{14}$	M + H	785.4681	785.4681	3.788	587.3925, 437.3402, 419.3302
9	5.12	Medicarpin	$C_{16}H_{14}O_4$	M + H	271.0964	271.0967	0.791	137.0578, 109.0631, 123.0423
10	5.41	Isolicoflavonol	$C_{20}H_{18}O_6$	M + H	355.1176	355.1173	-0.886	299.0536, 287.0539, 271.0582
11	5.95	Licochalcone a	$C_{21}H_{22}O_4$	M + H	339.159	339.1591	0.014	297.1461, 121.0282
12	6.6	Calycosin	$C_{16}H_{12}O_5$	M + H	285.0757	285.0753	-1.578	253.0511, 225.0541
13	6.61	Gancaonin A	$C_{21}H_{20}O_5$	M-H	351.1237	351.1236	2.563	351.1236, 237.0567
14	7.6	Licoisoflavanone	$C_{20}H_{18}O_6$	M + H	355.1176	355.1179	0.803	355.1179
15	7.66	Isoliquiritigenin	$C_{15}H_{12}O_4$	M-H	255.0662	255.0666	5.546	135.0086, 119.0508
16	7.86	Lupiwighteone	$C_{20}H_{18}O_5$	M + H	355.1176	355.1171	-1.45	355.1171
17	8.23	Eriodictyol	$C_{15}H_{12}O_6$	M + H	289.0706	289.0703	-1.261	271.0823, 253.1410
18	8.63	Formononetin	$C_{16}H_{12}O_4$	M + H	269.0808	269.0806	-0.875	139.0541, 89.0411
19	9.12	Ginsenoside F1	$C_{36}H_{62}O_9$	M + H	639.4466	639.4462	-6.188	459.3782, 441.3743
20	9.32	Saikosaponin D	$C_{42}H_{68}O_{13}$	M-H	779.4587	779.4585	-5.859	617.4001, 471.3465, 439.3227
21	9.46	Ginsenoside rh2	$C_{36}H_{62}O_8$	M + H	623.4517	623.4514	5.558	623.4514
22	10.33	Trametenolic acid	$C_{30}H_{48}O_3$	M + H	457.3676	457.3674	-0.485	439.3576
23	10.63	Kaempferol	$C_{15}H_{10}O_6$	M + H	287.055	287.0551	0.298	241.0491, 165.0181
24	11.18	Dehydroburicoic acid	$C_{31}H_{48}O_3$	M + H	469.3676	469.3677	6.67	469.3677, 451.3572
25	11.22	Quercetin	$C_{15}H_{10}O_7$	M + H	303.0499	303.0496	-1.086	285.039, 247.0596, 165.0183
26	12.01	Poricoic acid A	$C_{31}H_{46}O_5$	M + H	499.3418	499.3417	-11.764	481.3312, 463.3226

Table 1. Analysis of chemical composition of BZYQD by UPLC- MS/MS.

BZYQD inhibits CRC cell proliferation and migration via PI3K/Akt/mTOR axis inhibition

To explore the role of the PI3K/Akt/mTOR signaling pathway on anti-colorectal cancer effect of BZYQD, the PI3K inhibitors and agonists were utilized. Compared to the high-dose BZYQD group, the addition of a PI3K inhibitor further suppressed the proliferation and migration of HCT116 cells (Fig. 6A and D, $F_{3,8} = 55.772$, $P < 0.001$). Conversely, a PI3K agonist reversed the inhibitory effects of BZYQD on cell proliferation and migration. Further Western blot analysis showed that the PI3K inhibitor reduced the expression of p-mTOR ($F_{3,8} = 50.829$, $P < 0.001$), p-PI3K ($F_{3,8} = 213.615$ $P < 0.001$), and p-AKT ($F_{3,8} = 63.729$, $P < 0.001$, Fig. 7A and B), while the PI3K agonist reversed the inhibitory effects of BZYQD on the pathway (Fig. 7A and B). These findings underscore the crucial role of the PI3K/Akt/mTOR signaling pathway in BZYQD-mediated inhibition of CRC cell proliferation and migration.

BZYQD promoted CD86 levels and impeded CD206 levels in M1 macrophages

We further investigated the effects of BZYQD on macrophage polarization, focusing particularly on the PI3K/AKT/mTOR pathway. The type of RAW264.7 macrophages was shown in Fig. 8A and B. MTT assay were exploited to evaluate the effects of BZYQD on the viability of activated RAW264.7 macrophages (Fig. 8C). There was no significant difference between the viability of BZYQD treated cells and the control cells. Therefore, BZYQD concentrations of 165, 330, and 660 μg/mL were selected as the experimental dosages for subsequent experiments. CD86 and CD206 are recognized as surface markers for M1 and M2 macrophages, respectively. Flow cytometry (FCM) was employed to evaluate the impact of BZYQD on the expression of these markers (Fig. 8D and E). Stimulation with LPS plus IFN-γ resulted in an increase in the mean fluorescence intensity (MFI) of CD86 protein on M1 macrophages (Fig. 8D, $F_{5,12} = 241.896$, $P < 0.001$), while IL-4 stimulation significantly elevated CD206 protein levels on M2 macrophages compared to the control (Fig. 8E, $F_{5,12} = 15.275$, $P < 0.001$). The treatment with various concentrations of BZYQD led to a gradual increase in CD86 MFI on M1 cells, accompanied by a concentration-dependent decrease in CD206 MFI. This suggests that BZYQD promotes a enhancement in CD86 expression and an reduction in CD206 expression on M1 macrophages.

Moreover, IL-6 is predominantly released by M1 macrophages as a pro-inflammatory marker, whereas IL-10 is an anti-inflammatory cytokine produced by M2 macrophages. ELISA results shown in Fig. 8 indicate that levels of IL-6 released by M1 cells (Fig. 8F, $F_{5,12} = 388.341$, $P < 0.001$), and IL-10 by M2 cells, were significantly higher compared to the control group (Fig. 8G, $F_{5,12} = 59.198$, $P < 0.001$). Following co-incubation with BZYQD, the concentrations of IL-6 increased rapidly, whereas IL-10 levels gradually decreased compared to the control group (Fig. 8F and G). These findings illustrate that BZYQD influences macrophage polarization in vitro.

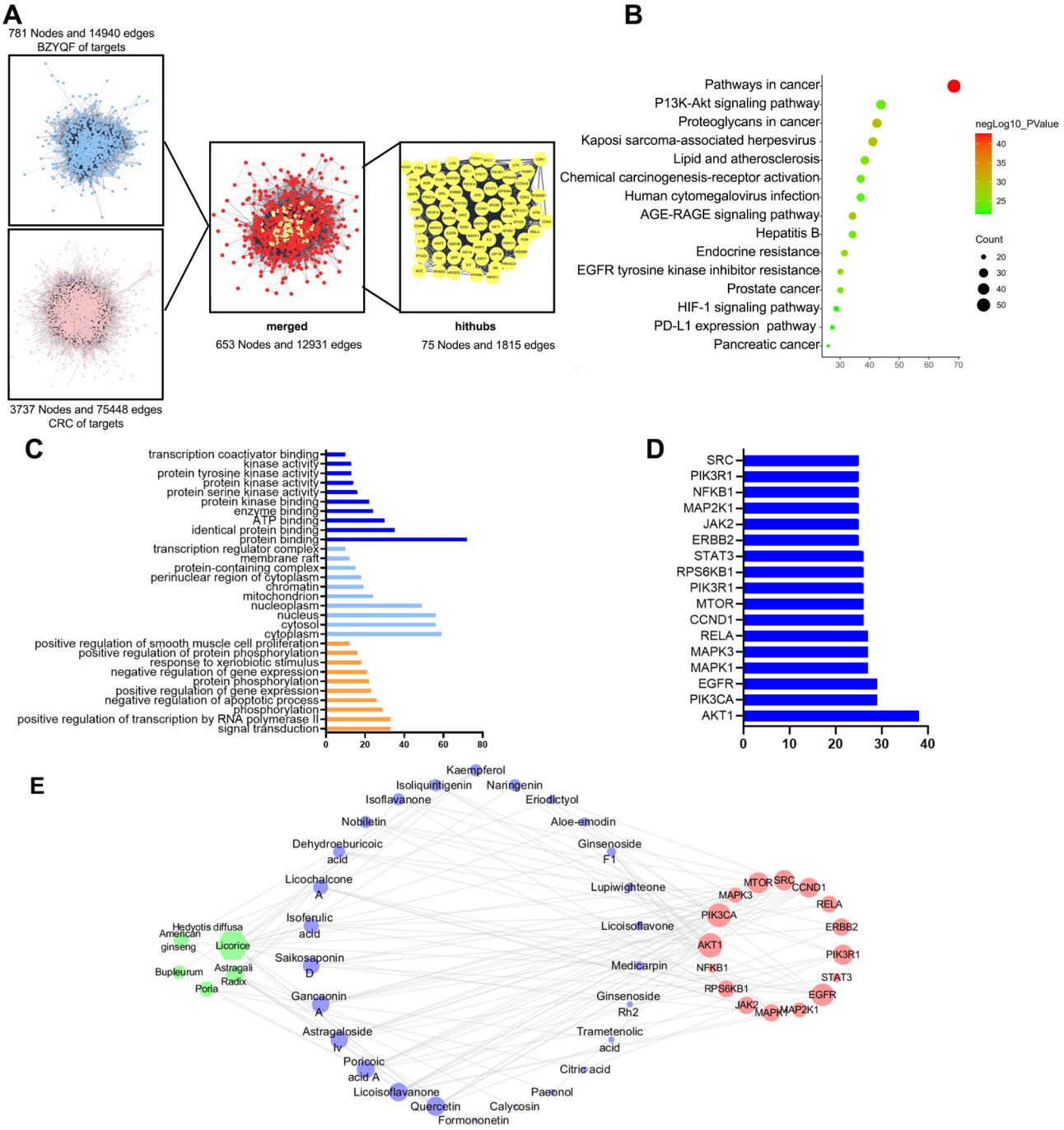

Fig. 2. Network pharmacology assessment of BZYQD on CRC: (**A**) The process of identifying core targets of BZYQD interacting with critical nodes in CRC. (**B**) A bubble chart illustrating the KEGG pathways analysis. (**C**) GO enrichment analysis. (**D**) The distribution of 17 key targets across the top 10 pathways. (**E**) Development of the key Chinese herbal medicines-components-targets network.

Discussion

The prevalence of colorectal cancer (CRC) has consistently been high in Western developed nations[15–17]. However, countries undergoing rapid development, such as China, are experiencing a shift in lifestyle and dietary patterns toward a more Westernized approach[15]. This transformation has brought factors like CRC, sedentary behavior, and high-fat diets into greater focus, contributing to a yearly rise in CRC incidence and placing a significant economic strain on healthcare[18]. CRC is a complex disease influenced by lifestyle choices, genetic predispositions, and environmental factors[18]. Typically, colorectal adenomas can progress to CRC over a period of 10 to 15 years[19]. The clinical symptoms of CRC are varied and often nonspecific, including rectal bleeding, alterations in bowel habits, and abdominal discomfort[16]. Early detection largely relies on endoscopic

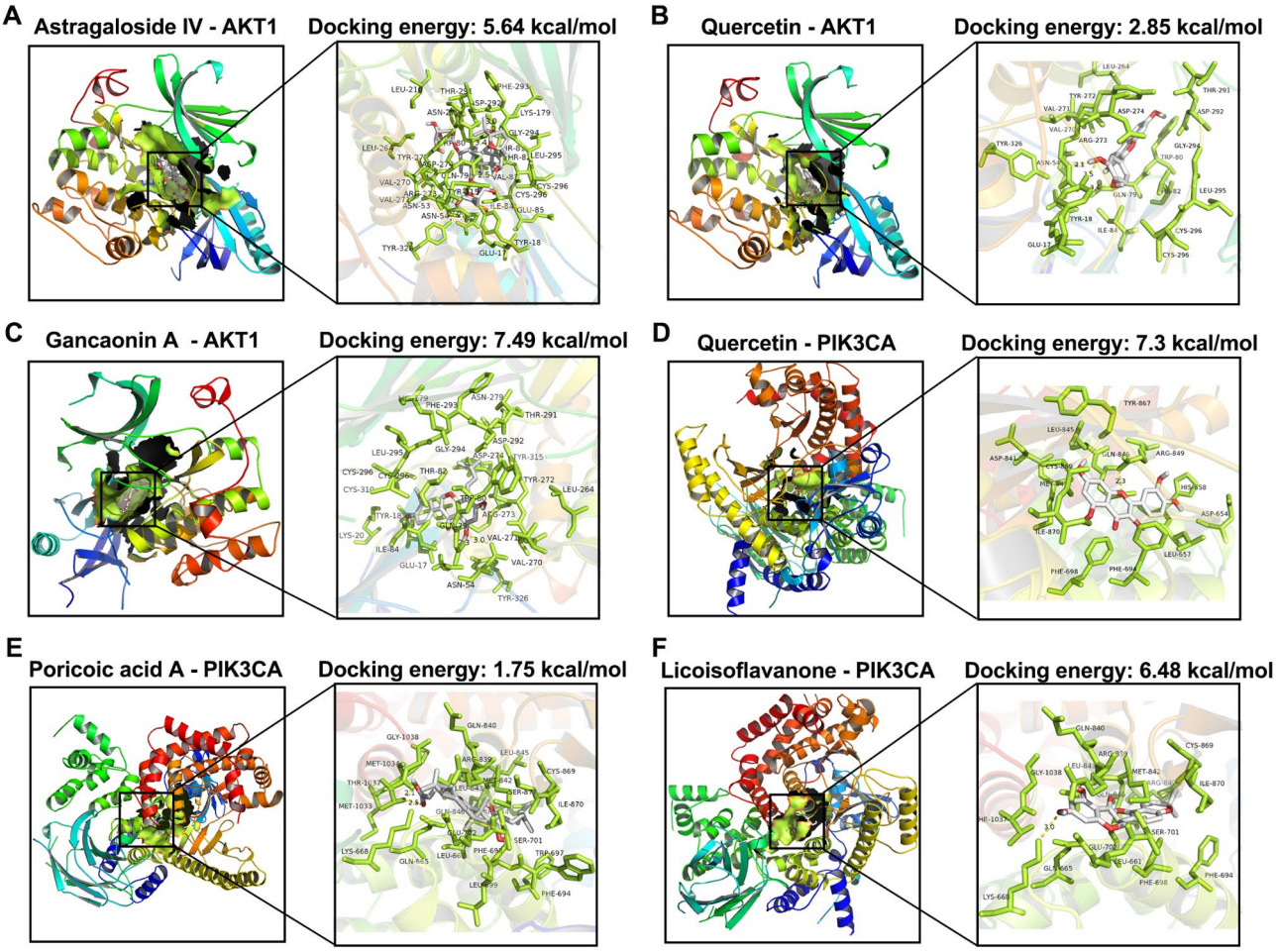

Fig. 3. Molecular models of astragaloside IV, gancaonin A, poricoic acid A, quercetin, and licoisoflavanone binding to its predicted protein targets: (A-F)

procedures, as up to 50% of patients may present with metastatic tumors at the time of initial diagnosis, with liver metastasis being the most prevalent form (50%)[20]. Current treatment options encompass endoscopic and surgical resections, chemotherapy, radiotherapy, targeted biological therapies, and immunotherapy[20]. Thanks to advancements in CRC treatments, the survival duration for patients with advanced stages of the disease has improved from approximately 5 months to around 30 months, although each treatment modality is associated with its own unique side effects and complications[17].

Traditional Chinese Medicine (TCM) offers distinct benefits in managing colorectal cancer (CRC)[21,22]. It promotes apoptosis in tumor cells while also suppressing their proliferation[23]. TCM can be utilized independently or alongside chemotherapy to address advanced CRC and has proven effective during both postoperative recovery and radiochemotherapy phases[24]. Its applications include alleviating postoperative complications[24]. TCM practitioners adjust dosages based on individual patient conditions and symptoms, leading to variability in treatment[25]. Modern medicine has identified numerous monomeric compounds in BZYQD, such as astragaloside IV[26], ginsenosides[27], atractylenolides[28], and quercetin[29], which exhibit anti-CRC properties. Their mechanisms may involve the inhibition of abnormal cell proliferation in colonic mucosa, reduction of inflammation and neovascularization, and regulation of intestinal flora[28,29]. Additionally, the polysaccharide found in Fu Ling can mitigate the intestinal damage caused by 5-fluorouracil (5-FU) and help regulate the intestinal microbiome[30].

In this study, a network pharmacology approach was used to explore the mechanisms underlying the effects of BZYQD on CRC in vitro. As it is composed of several different herbs, BZYQD is complex. Through network pharmacology analysis, we established a network linking the BZYQD compound to its therapeutic targets, identifying a total of 146 targets. Further analysis of the PPI network revealed that the top targets with the highest connectivity included AKT1, PIK3CA, EGFR, MAPK1, MAPK3, and RELA. Integrating findings from GO and KEGG analyses, we determined that the primary target of BZYQD is the PI3K/AKT signaling pathway. The PI3K family consists of three isoforms, each characterized by distinct structures and functions, with PI3KI being the most extensively characterized. This isoform forms a heterodimer comprising a regulatory subunit and a catalytic subunit. PI3K is triggered by growth factor receptor signaling, serving as a second messenger that mediates signals to various cellular targets[31]. AKT, a serine/threonine kinase with three isoforms, is activated by signals relayed from PI3K, which converts input from various upstream cytokines and growth factors into

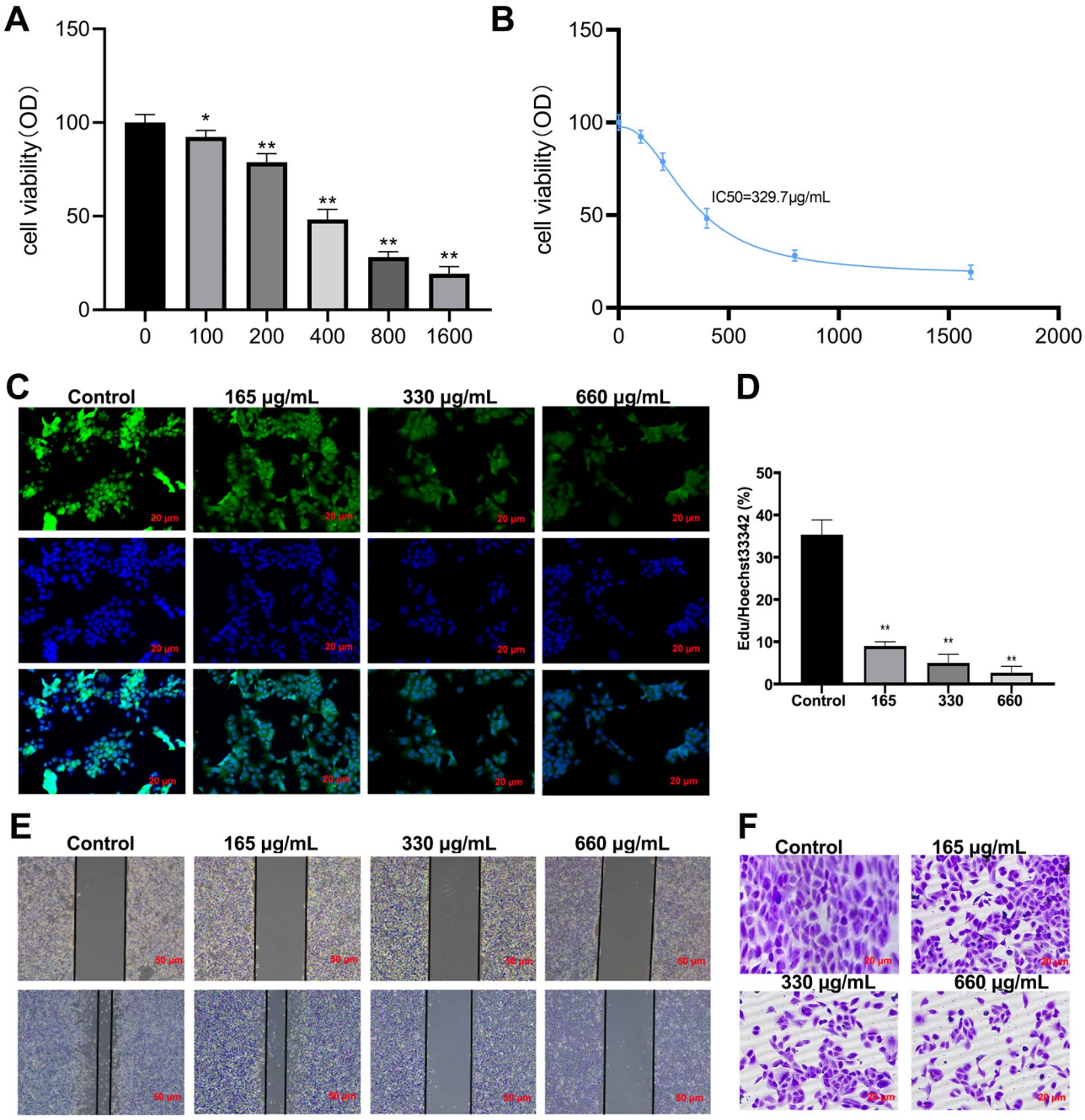

Fig. 4. Impact of BZYQD on the proliferation and migration of HCT116 cells in vitro. (**A, B**) HCT116 cells were exposed to a blend of BZYQD at concentrations of 0, 100, 200, 400, 800, and 1600 μg/ml. An MTT assay was conducted to evaluate cell viability, and IC50 values were determined. Additionally, HCT116 cells were treated with the primary components of BZYQD at concentrations of 165, 330, and 660 μg/ml. (**C, D**) Cell proliferation was assessed using EdU labeling, with DNA stained blue and proliferating cells stained green. (**E**) The migratory capacity of HCT116 cells was analyzed through a wound healing assay. (**F**) A Transwell migration assay was also employed to assess the migration ability of HCT116 cells. The data are expressed as mean ± SEM ($n = 3$). $^{*}P < 0.05$ and $^{**}P < 0.01$ in comparison to the control group.

actionable information for AKT and its downstream pathways. AKT, in turn, activates the mTOR complex 1, which is sensitive to rapamycin[32]. The PI3K/AKT/mTOR pathway plays a critical role in numerous physiological and pathological processes, including cell growth, proliferation, metabolism, protein and lipid synthesis, and autophagy[33]. Numerous studies have demonstrated that this pathway is often aberrantly activated in various cancers, including colorectal cancer (CRC)[34]. Consequently, several anti-CRC drugs targeting the PI3K/AKT/mTOR pathway have been developed and proven effective. Building on these insights, we conducted both in vitro experiments to validate our hypotheses. Initially, HCT116 cells were treated with a combination of

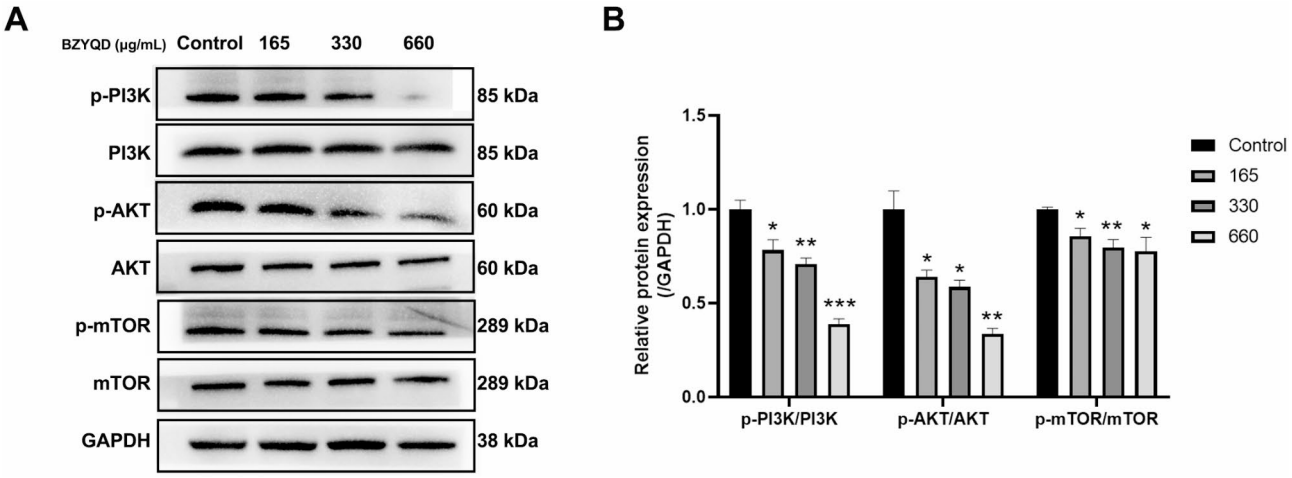

Fig. 5. Expression of PI3K/AKT/mTOR pathway protein (**A, B**). The data are expressed as mean ± SEM ($n = 3$). $^{*}P < 0.05$ and $^{**}P < 0.01$ in comparison to the control group.

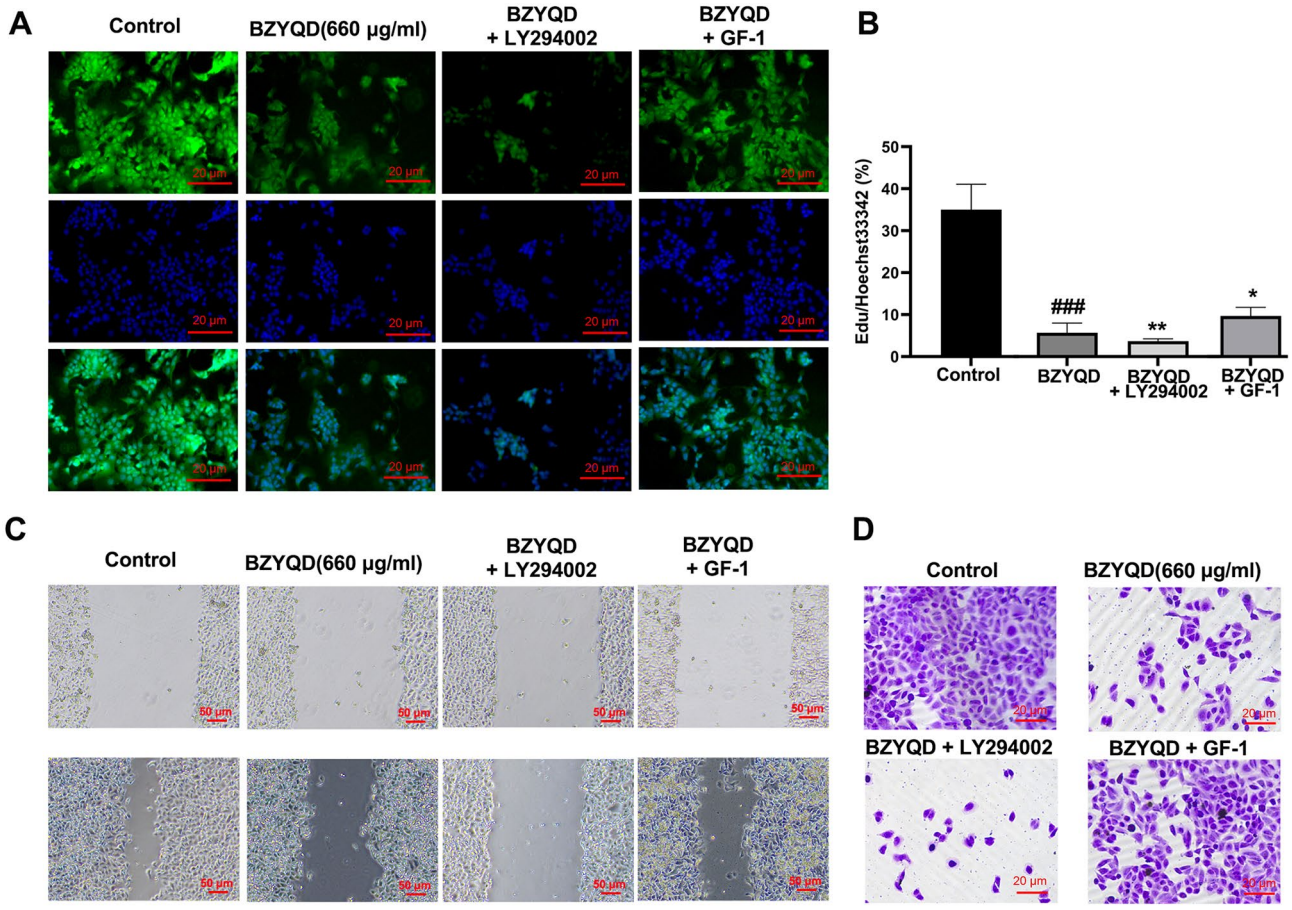

Fig. 6. BZYQD inhibits crc cell proliferation and migration via PI3K/Akt/mTOR axis inhibition. (**A, B**) The impact of BZYQD, LY294002, and IGF-1 on CRC cell proliferation (DNA stained blue and proliferating cells marked in green). (**C, D**) The influence of BZYQD, LY294002, and IGF-1 on CRC cell migration. Data are expressed as mean ± SEM ($n = 3$). $^{**}P < 0.01$ vs. the Con group, $\#\#P < 0.01$ vs. the BZYQD group.

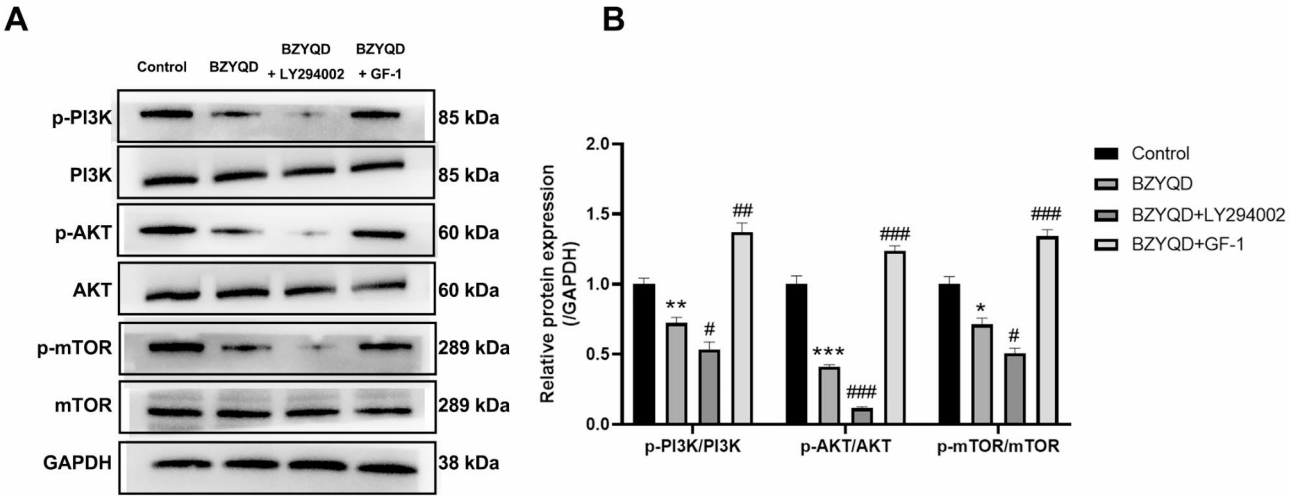

Fig. 7. Impact of BZYQD, LY294002, and IGF-1 on PI3K/AKT/mTOR pathway protein expression in CRC (**A, B**). Data are expressed as mean ± SEM ($n = 3$). $^{**}P < 0.01$ vs. the Con group, $^{\#\#}P < 0.01$ vs. the BZYQD group.

the primary components of BZYQD, resulting in a significant inhibition of cell proliferation and migration. Additionally, the phosphorylation levels of PI3K, AKT, and mTOR were notably reduced in HCT116 cells treated with the BZYQD component mixture. Nevertheless, the BZYQD in this study has a relatively high IC50 of 329.7 μg/ml. Traditional Chinese medicine often demonstrates more pronounced pharmacological effects at higher doses; however, it is essential to remain vigilant regarding potential adverse reactions. Wang et al. selected concentrations of 150, 304, and 600 μg/ml of Banxia Xiexin Decoction (BXD) as low, medium, and high doses in CRC studies, confirmed that the primary components of BXD significantly inhibited the proliferation of HCT116 cells[35]. Shang et al. reported that Sijunzi Decoction (SJZD) at concentrations of 50, 70, and 100 μg/ml could induce apoptosis in HCT116 cells[36]. Meanwhile, Lu et al. evaluated the effects of varying concentrations (0, 1, 2, 4 mg/ml) of Bazhen Decoction (BZD) on the invasion capacity and apoptotic rate of CRC cell lines. The results indicated that BZD exhibited a dose-dependent suppression of CRC cell invasion and promoted apoptosis in CRC cells[37]. Therefore, high doses of traditional Chinese medicine may yield more effective results in in-vitro colon cancer experiments. In this study, although we found that the five active ingredients of BZYQD—astragaloside IV, gancaonin A, quercetin, poricoic acid A, and licoisoflavanone—have lower IC50 values, the safety and efficacy of BZYQD require further verification through animal experiments. Additionally, BZYQD is currently being used in the clinical treatment of CRC, administered at a dosage of 60 g/day for a duration of 1 to 2 months[38]. Compared to the chemotherapy group, BZYQD combined with chemotherapy has been shown to enhance patient survival rates and quality of life, demonstrating high safety and warranting clinical promotion and implementation[38]. Therefore, BZYQD holds significant promise for clinical application. More importantly, an in-depth investigation into its safety profile is imperative.

In the tumor microenvironment, the balance between M1 and M2 macrophages plays a crucial role in tumor development and treatment[39]. Studies have shown that changes in the M1/M2 ratio may be related to tumor progression and prognosis[40]. M1 macrophages are generally considered antitumor due to their ability to inhibit tumor cell growth and metastasis and to enhance specific immune responses[40]. In contrast, M2 macrophages are often associated with tumor promotion. They can promote the proliferation, invasion, and metastasis of tumor cells by inhibiting the immune response[41]. Additionally, M2 macrophages can facilitate angiogenesis, providing essential nutrients and oxygen to the tumor[41]. Inhibition of the PI3K/AKT/mTOR signaling pathway usually promotes the polarization of M1 macrophages and enhances their inflammatory response[42]. From this research, we observed that the M1 phenotype can be induced in RAW264.7 macrophages through LPS and IFN-γ treatment, resulting in significant changes in cellular morphology and increased levels of apoptosis. Additionally, there was an upregulation of M1-type inflammatory mediators such as IL-6 and CD86. Conversely, the M2 phenotype could be induced with IL-4, leading to a rise in anti-inflammatory factors like IL-10 and CD206, indicating the successful establishment of macrophage inflammatory models. Following treatment with BZYQD, the levels of proinflammatory cytokines in M1-polarized RAW264.7 cells were increased reduced, while the levels of anti-inflammatory molecules reduced. Specifically, there was a increase in IL-6 secreted by M1 cells and a notable decrease in IL-10 secreted by M2 cells. These findings suggest that BZYQD promotes the polarization of M1 macrophages, and inhibits tumor cell growth and metastasis.

Conclusion

Our results indicate that BZYQD inhibits colon cancer proliferation and migration by modulating the PI3K/Akt/mTOR signaling pathway in CRC. This highlights BZYQD as a promising adjuvant for CRC treatment.

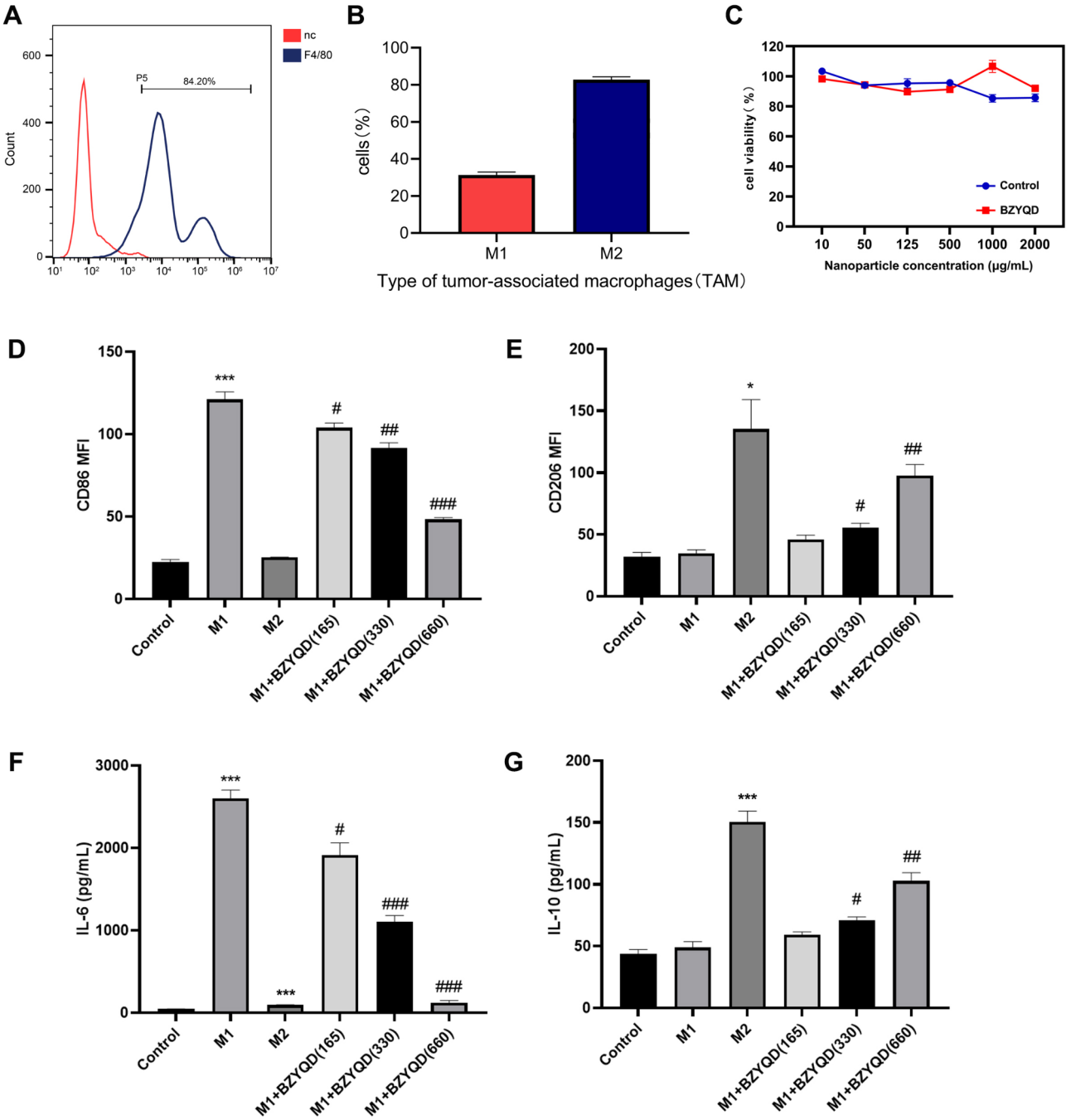

Fig. 8. BZYQD impeded CD86 levels and promoted CD206 levels in M1 macrophages. (**A, B**) Flow cytometry was utilized for both qualitative and quantitative analysis of tumor-associated macrophages (TAMs). (**C**) The cytotoxic effect of BZYQD on TAMs following 24 h of treatment was assessed in vitro using a CCK-8 assay. (**D, E**) The analysis shows the mean fluorescence intensity (MFI) with histograms for CD86 MFI and CD206 MFI. (**F, G**) The impact of BZYQD on the secretion of IL-6 and IL-10 in activated macrophages was evaluated. Data are expressed as mean ± SEM ($n = 3$). $^{**}P < 0.01$ vs. the Con group, $^{\#\#}P < 0.01$ vs. the M1 group.

Data availability

The datasets used and/or analysed during the current study available from the corresponding author on reasonable request.

Received: 16 November 2024; Accepted: 3 February 2025
Published online: 10 March 2025

References

1. Dekker, E., Tanis, P. J., Vleugels, J. L. A., Kasi, P. M. & Wallace, M. B. Colorectal cancer. *Lancet (London England)*. **394** (10207), 1467–1480 (2019).
2. Eng, C. et al. A comprehensive framework for early-onset colorectal cancer research. *Lancet Oncol.* **23** (3), e116–e128 (2022).
3. DeCosse, J. J., Tsioulias, G. J. & Jacobson, J. S. Colorectal cancer: Detection, treatment, and rehabilitation. *Cancer J. Clin.* **44** (1), 27–42 (1994).
4. Li, Q. et al. Signaling pathways involved in colorectal cancer: Pathogenesis and targeted therapy. *Signal. Transduct. Target. Therapy*. **9** (1), 266 (2024).
5. Gou, H. et al. Traditional Medicine Pien Tze Huang suppresses colorectal tumorigenesis through restoring gut microbiota and metabolites. *Gastroenterology* **165** (6), 1404–1419 (2023).
6. Hua, Z. et al. Deciphering the protective effect of Buzhong Yiqi Decoction on osteoporotic fracture through network pharmacology and experimental validation. *J. Orthop. Surg. Res.* **18** (1), 86 (2023).
7. Hu, R. et al. Jiawei Buzhong Yiqi decoction ameliorates polycystic ovary syndrome via oocyte-granulosa cell communication. *J. Ethnopharmacol.* **323**, 117654 (2024).
8. Hu, J., Li, X., Fang, Y. & Peng, J. Efficacy and safety of Buzhong Yiqi Decoction in improving cancer-related fatigue and immunity of cervical carcinoma patients: A protocol of randomized controlled trial. *Medicine* **100** (49), e27938. (2021).
9. Zeng, P. et al. Integrating network pharmacology and experimental verification to investigate the pharmacological mechanisms of Buzhong Yiqi decoction in the treatment of non-small cell lung cancer. *Chem. Biol. Drug Des.* **103** (1), e14414. (2024).
10. Hu, Q., Chen, X. P., Tang, Z. J., Zhu, X. Y. & Liu, C. Therapeutic effects of Buzhong Yiqi decoction in patients with spleen and stomach qi deficiency after routine surgery and chemotherapy for colorectal cancer. *World J. Gastrointest. Surg.* **16** (7), 2183–2193 (2024).
11. Nogales, C. et al. Network pharmacology: Curing causal mechanisms instead of treating symptoms. *Trends Pharmacol. Sci.* **43** (2), 136–150 (2022).
12. Zhang, P. et al. Network pharmacology: Towards the artificial intelligence-based precision traditional Chinese medicine. *Brief. Bioinform.* **25** (1). (2023).
13. Zhao, L. et al. Network pharmacology, a promising approach to reveal the pharmacology mechanism of Chinese medicine formula. *J. Ethnopharmacol.* **309**, 116306 (2023).
14. Bai, G. et al. Research advances of molecular docking and molecular dynamic simulation in recognizing interaction between muscle proteins and exogenous additives. *Food Chem.* **429**, 136836 (2023).
15. Shin, A. E., Giancotti, F. G. & Rustgi, A. K. Metastatic colorectal cancer: Mechanisms and emerging therapeutics. *Trends Pharmacol. Sci.* **44** (4), 222–236 (2023).
16. Wong, S. H. & Yu, J. Gut microbiota in colorectal cancer: Mechanisms of action and clinical applications. *Nat. Rev. Gastroenterol. Hepatol.* **16** (11), 690–704 (2019).
17. Gupta, S., May, F. P., Kupfer, S. S. & Murphy, C. C. Birth cohort Colorectal Cancer (CRC): Implications for Research and Practice. *Clin. Gastroenterol. Hepatol. Off. Clin. Pract. J. Am. Gastroenterol. Assoc.* **22** (3), 455–469e7 (2024).
18. Biller, L. H. & Schrag, D. Diagnosis and treatment of metastatic colorectal Cancer: A review. *Jama* **325** (7), 669–685 (2021).
19. Mármol, I., Sánchez-de-Diego, C., Pradilla Dieste, A., Cerrada, E. & Rodriguez Yoldi, M. J. Colorectal carcinoma: A General Overview and Future perspectives in Colorectal Cancer. *Int. J. Mol. Sci.* **18** (1). (2017).
20. Yan, H., Talty, R. & Johnson, C. H. Targeting ferroptosis to treat colorectal cancer. *Trends Cell Biol.* **33** (3), 185–188 (2023).
21. Cai, K. et al. Xianlian Jiedu Decoction alleviates colorectal cancer by regulating metabolic profiles, intestinal microbiota and metabolites. *Phytomed. Int. J. Phytother. Phytopharmacol.* **128**, 155385 (2024).
22. Sui, H. et al. YYFZBJS ameliorates colorectal cancer progression in apc(Min/+) mice by remodeling gut microbiota and inhibiting regulatory T-cell generation. *Cell. Commun. Signal. CCS.* **18** (1), 113 (2020).
23. Wang, F. et al. Targeting VCP potentiates immune checkpoint therapy for colorectal cancer. *Cell. Rep.* **42** (11), 113318 (2023).
24. Mao, Q. et al. Self-assembled traditional Chinese nanomedicine modulating tumor immunosuppressive microenvironment for colorectal cancer immunotherapy. *Theranostics* **12** (14), 6088–6105 (2022).
25. Sun, Q. et al. Traditional Chinese medicine and colorectal cancer: Implications for drug discovery. *Front. Pharmacol.* **12**, 685002 (2021).
26. Wang, S., Mou, J., Cui, L., Wang, X. & Zhang, Z. Astragaloside IV inhibits cell proliferation of colorectal cancer cell lines through down-regulation of B7-H3. *Biomed. Pharmacother. Biomed. Pharmacother.* **102**, 1037–1044 (2018).
27. Zhao, L. et al. Therapeutic effects of ginseng and ginsenosides on colorectal cancer. *Food Funct.* **13** (12), 6450–6466 (2022).
28. Wu, Y. et al. Atractylenolide II combined with Interferon-γ synergistically ameliorates colorectal cancer progression in vivo and in vitro by blocking the NF-kB p65/PD-L1 pathway. *J. Cancer*. **15** (13), 4328–4344 (2024).
29. Sun, D. et al. A cyclodextrin-based nanoformulation achieves co-delivery of ginsenoside Rg3 and quercetin for chemo-immunotherapy in colorectal cancer. *Acta Pharm. Sin. B*. **12** (1), 378–393 (2022).
30. Wang, C., Yang, S., Gao, L., Wang, L. & Cao, L. Carboxymethyl pachyman (CMP) reduces intestinal mucositis and regulates the intestinal microflora in 5-fluorouracil-treated CT26 tumour-bearing mice. *Food Funct.* **9** (5), 2695–2704 (2018).
31. Stefani, C. et al. PI3K/AKT/mTOR and MAPK signaling pathways in Colorectal Cancer Pathogenesis: Where are we now? *Int. J. Mol. Sci.* **22**, 19 (2021).
32. Jiang, T. et al. CircIL4R activates the PI3K/AKT signaling pathway via the miR-761/TRIM29/PHLPP1 axis and promotes proliferation and metastasis in colorectal cancer. *Mol. Cancer*. **20** (1), 167 (2021).
33. Dong, S. et al. ROS/PI3K/Akt and Wnt/β-catenin signalings activate HIF-1α-induced metabolic reprogramming to impart 5-fluorouracil resistance in colorectal cancer. *J. Exp. Clin. Cancer Res. CR.* **41** (1), 15 (2022).
34. Duan, S. et al. IMPDH2 promotes colorectal cancer progression through activation of the PI3K/AKT/mTOR and PI3K/AKT/FOXO1 signaling pathways. *J. Exp. Clin. Cancer Res. CR.* **37** (1), 304 (2018).
35. Wang, Y. et al. Effect and mechanism of Banxia Xiexin decoction in colorectal cancer: A network pharmacology approach. *Phytomed. Int. J. Phytother. Phytopharmacol.* **123**, 155174 (2024).
36. Shang, L. et al. Mechanism of Sijunzi Decoction in the treatment of colorectal cancer based on network pharmacology and experimental validation. *J. Ethnopharmacol.* **302**, 115876 (2023). (Pt A).
37. Lu, S. et al. Mechanism of Bazhen decoction in the treatment of colorectal cancer based on network pharmacology, molecular docking, and experimental validation. *Front. Immunol.* **14**, 1235575 (2023).
38. Jianan, Q., Yan, X. U., Hongyi, H. U. & Aiguang, Z. Clinical efficacy and safety evaluation of Buzhongyiqi pills on appetite improvement in patients with colorectal cancer receiving chemotherapy: A pilot randomized cross-over clinical trial. *J. Tradit. Chin. Med. = Chung i tsa Chih Ying Wen pan.* **44** (6), 1254–1267 (2024).
39. Zhao, S. et al. Tumor-derived exosomal miR-934 induces macrophage M2 polarization to promote liver metastasis of colorectal cancer. *J. Hematol. Oncol.* **13** (1), 156 (2020).
40. Li, R. et al. Gut microbiota-stimulated cathepsin K secretion mediates TLR4-dependent M2 macrophage polarization and promotes tumor metastasis in colorectal cancer. *Cell Death Differ.* **26** (11), 2447–2463 (2019).
41. Lu, S. et al. A novel tRNA-derived fragment tRF-3022b modulates cell apoptosis and M2 macrophage polarization via binding to cytokines in colorectal cancer. *J. Hematol. Oncol.* **15** (1), 176 (2022).

42. Zhang, Z. et al. Retinal microenvironment-protected Rhein-GFFYE nanofibers attenuate retinal ischemia-reperfusion Injury via inhibiting oxidative stress and regulating Microglial/Macrophage M1/M2 polarization. *Adv. Sci. (Weinheim Baden-Wurttemberg Germany)*. **10** (30), e2302909 (2023).

Acknowledgements
None.

Author contributions
Song Qiao and Wanling Lu contributed equally to this work. Conceptualization: Xiaolong Li and Shangzhen Yang. Methodology: Hua Hua and Chengtao Mao. Software and validation: Song Qiao. Writing–original draft preparation: Song Qiao and Wanling Lu. Writing–review and editing: Song Qiao and Wanling Lu. Visualization: Xiaolong Li and Shangzhen Yang. Supervision: Song Qiao. All authors read and approved the ffnal version of the manuscript.

Declarations

Competing interests
The authors declare no competing interests.

Additional information
Supplementary Information The online version contains supplementary material available at https://doi.org/10.1038/s41598-025-89018-9.

Correspondence and requests for materials should be addressed to W.L.

Reprints and permissions information is available at www.nature.com/reprints.

Publisher's note Springer Nature remains neutral with regard to jurisdictional claims in published maps and institutional affiliations.